Published in final edited form as:
EMBO Mol Med. 2010 July ; 2(7): 258–274. doi:10.1002/emmm.201000079.

Caseation of Human Tuberculosis Granulomas Correlates with Elevated Host Lipid Metabolism

Mi-Jeong Kim[1], **Helen C. Wainwright**[2], **Michael Locketz**[2], **Linda-Gail Bekker**[3], **Gabriele B. Walther**[4,5], **Corneli Dittrich**[2], **Annalie Visser**[2], **Wei Wang**[6], **Fong-Fu Hsu**[7], **Ursula Wiehart**[1,8], **Liana Tsenova**[9], **Gilla Kaplan**[9], and **David G. Russell**[1,*]

Mi-Jeong Kim: mk376@cornell.edu; Helen C. Wainwright: Helen.Wainwright@uct.ac.za; Michael Locketz: Michael.Locketz@uct.ac.za; Linda-Gail Bekker: Linda-Gail.Bekker@hiv-research.org.za; Gabriele B. Walther: walther.gabi@gmail.com; Corneli Dittrich: Corneli.Dittrich@uct.ac.za; Annalie Visser: Annalie.Visser@uct.ac.za; Wei Wang: ww77@cornell.edu; Fong-Fu Hsu: FHSU@DOM.wustl.edu; Liana Tsenova: tsenovli@umdnj.edu; Gilla Kaplan: kaplangi@umdnj.edu

[1] Department of Microbiology and Immunology, College of Veterinary Medicine, Cornell University, Ithaca, NY 14850, USA

[2] Division of Anatomical Pathology, University of Cape Town Faculty of Health Sciences, Cape Town, South Africa

[3] The Desmond Tutu HIV Centre, Institute of Infectious Disease and Molecular Medicine, Department of Medicine, University of Cape Town, Cape Town, South Africa

[4] Chris Barnard Division of Cardio-Thoracic Surgery, Groote Schuur Hospital, University of Cape Town, Cape Town, South Africa

[6] Department of Biomedical Sciences, College of Veterinary Medicine, Cornell University, Ithaca, NY 14850, USA

[7] Department of Internal Medicine, Washington University School of Medicine, St. Louis, MO 63110, USA

[9] Laboratory of Mycobacterial Immunity and Pathogenesis, Public Health Research Institute Center at UMDNJ, Newark, NJ 07103, USA

Abstract

The progression of human tuberculosis to active disease and transmission involves the development of a caseous granuloma that cavitates and releases infectious *Mycobacterium tuberculosis* bacilli. In the current study, we exploited genome-wide microarray analysis to determine that genes for lipid sequestration and metabolism were highly expressed in caseous tuberculosis granulomas. Immunohistological analysis of these granulomas confirmed the disproportionate abundance of the proteins involved in lipid metabolism in cells surrounding the caseum; namely, adipophilin, acyl-CoA synthetase long-chain family member 1, and saposin C. Biochemical analysis of the lipid species within the caseum identified cholesterol, cholesteryl esters, triacylglycerols, and lactosylceramide, which implicated low-density lipoprotein-derived lipids as the most likely source. *M. tuberculosis* infection *in vitro* induced lipid droplet formation in murine and human macrophages. Furthermore, the *M. tuberculosis* cell wall lipid, trehalose dimycolate, induced a strong granulomatous response in mice, which was accompanied by foam

[*]Corresponding author: David G. Russell (dgr8@cornell.edu), Tel 607 253 3401, FAX 607 253 4058.
[5]Current Address: Department for General, Abdominal, Vascular and Thoracic Surgery, Klinikum Bogenhausen, Teaching Hospital of the TU München, Munich, Germany
[8]Current Address: Medical Biosciences Department, University of the Western Cape, Private Bag X17, Bellville, 7535, South Africa, uwiehart@uwc.ac.za

cell formation. These results provide molecular and biochemical evidence that the development of the human tuberculosis granuloma to caseation correlates with pathogen-mediated dysregulation of host lipid metabolism.

INTRODUCTION

Despite advances in modern medicine, tuberculosis (TB) still remains one of the most deadly infectious diseases with about 8 million infected individuals progressing to active disease and about 2 million people dying of TB annually (Dye, Bassili et al. 2008). The synergy between HIV and *Mycobacterium tuberculosis* (Mtb) infections is a cause for considerable concern, and TB has emerged as the diagnostic infection for the progression to acquired immunity deficiency syndrome (AIDS) in sub-Saharan Africa.

Shortly after Mtb infection, the tissue site becomes organized into a granuloma, which comprises of a core of infected macrophages surrounded by foamy and epithelioid macrophages, monocytes, and multinucleated giant cells (MGCs) (Russell 2007). The periphery of the granuloma is marked by fibroblasts that lay down a fibrous capsule around the macrophage-rich center. Once the capsule has formed, lymphocytes are scarce within the granuloma center and are most abundant at the periphery of granuloma. In this state, the granuloma represents a stable structure that maintains a fairly constant bacterial load but does not cause any overt signs of disease in the infected individual. Progression of the latent TB towards active disease correlates with the increased accumulation of caseum in granulomas, which is thought to result from the death of macrophages in the granuloma center (Dannenberg and Sugimoto 1976; Dannenberg 1994; Russell, Cardona et al. 2009). The granuloma becomes increasingly necrotic until the center liquefies and ruptures into the lung airway. At this late stage, many of the Mtb bacilli are extracellular and free bacilli are released into the airways to be exhaled into the atmosphere, thus facilitating spread of the infection.

Progression of disease is determined locally at the level of the granuloma; however, the factors that lead to granuloma development remain to be determined. Progression to active disease is almost universally regarded as a “failure” of the host immune system to control the infection. However, this is a “host-centered” view that minimizes Mtb’s ability to manipulate the host response locally and to induce the damage that is required for the pathogen to complete its life cycle. Recent data on granuloma model systems have revealed how Mtb is extremely adept at inducing responses that lead to extensive tissue remodeling and pathology (Actor, Olsen et al. 2001; Karakousis, Yoshimatsu et al. 2004; Puissegur, Botanch et al. 2004; Geisel, Sakamoto et al. 2005; Rhoades, Geisel et al. 2005). These data indicate that Mtb actively modulates the localized tissue response throughout the course of infection. Despite the critical importance of understanding the changes in tissue metabolism within TB granuloma, few studies have looked beyond immune mechanisms to probe the underlying pathology required to generate active disease.

In the current study, we exploited laser capture microdissection (LCM) and genome-wide microarray analysis to investigate human TB granulomas. Amongst several physiological changes revealed by transcriptional profiling, we noted that host genes for lipid sequestration and metabolism, namely, adipophilin (*ADFP*), acyl Co-A synthase long chain family member 1 (*ACSL1*), and prosaposin (*PSAP*), were upregulated in caseous human pulmonary TB granulomas. Immunohistological analysis of human TB granulomas confirmed the disproportionate abundance of ADFP, ACSL1, and the PSAP product, saposin C (SapC), in cells surrounding the caseum. Biochemical analysis of the major lipid species within the caseum revealed an abundance of cholesterol ester (CE), cholesterol

(CHO), and triacylglycerol (TAG), and also a high level of lactosylceramide (LacCer), which is known to influence both CHO sequestration and cell death (Chatterjee, Dey et al. 1997; Garner, Mellor et al. 2002). Mtb bacilli induced similar lipid sequestration and foam cell formation in murine and human macrophages *in vitro*. Significantly, using a murine granuloma model we developed previously (Rhoades, Geisel et al. 2005), we observed that the Mtb cell wall lipid trehalose dimycolate (TDM) injected with Matrigel into the subcutis of mice induced a strong granulomatous response and extensive foam cell formation.

The data presented here provide compelling evidence that the development of the lipid-rich caseum in the human TB granuloma correlates with a re-alignment in host lipid metabolism within the granuloma. The induction of a similar response by the bacterial lipid TDM implies that this is a pathogen-driven response, which results in a metabolic shift that induces the pathology necessary for the pathogen to complete its life cycle.

RESULTS

Transcriptional Profiling of Caseous Human Pulmonary TB Granulomas

Previous studies of the human response to Mtb infection at the molecular level have examined the gene expression profiles of bronchoalveolar lavage fluid (BALF) samples, peripheral blood mononuclear cells (PBMCs), human cell lines, or human TB lesions by using quantitative real-time RT-PCR and/or microarray for a subset of genes (Ragno, Romano et al. 2001; Zhu, Xiao et al. 2003; Grassi, Bocchino et al. 2006; Kim, Park et al. 2006; Ulrichs and Kaufmann 2006; Volpe, Cappelli et al. 2006). Although these studies have provided valuable information, we feel that characterization of global gene expression within human pulmonary TB granulomas is required to further our appreciation of the disease process. In the current study, lung tissues were surgically excised from TB patients with extensive lung cavitation and tissue degeneration, and laser-capture microdissection (LCM) was employed to dissect out granulomas, excluding uninvolved lung tissue. We specifically selected caseous granulomas for this study because accumulation of caseum is a histologically-defined process that is correlative of granuloma liquefaction and cavitation, which leads ultimately to transmission (Fig S1) (Dannenberg and Sugimoto 1976; Dannenberg 1994). Total RNAs were extracted from LCM samples, and mRNAs were amplified, biotin-labeled and hybridized on to genome-wide Human X3P array that is specifically designed based on 200 base pairs towards 3′ end of mRNA.

We analyzed the array data in two different ways. Firstly, selection of an appropriate control is problematic because the TB granuloma is strikingly different from uninfected lung parenchyma and contains a markedly different set of cell lineages; therefore the comparison between infected and uninfected tissue is of debatable value. In addition, there is no justification to biopsy healthy lung tissue, so we are limited to uninvolved lung tissue from TB patients. Nonetheless, we did generate an array profile from “normal”, uninvolved lung parenchyma to include as a control and used this to produce a relative list of transcripts from caseous granulomas compared to the normal lung tissue sample (GEO Accession# GSE20050, Table SII). Secondly, we generated a hierarchical list of absolute transcript abundance from caseous granulomas (GEO Accession# GSE20050, Table SI), in case the comparative list generated misleading results. Fortunately, both the comparative and hierarchical array lists showed very similar rankings of transcript abundance.

Preliminary examination of granuloma-associated abundant transcripts identified gene subsets involved in a number of destructive tissue pathologies such as invasive cancers and metabolic diseases, suggesting overlap in pathological mechanisms (Tuomisto and Yla-Herttuala 2005; Bild, Yao et al. 2006; Ma, Dahiya et al. 2009). However, we focused on lipid metabolism as previous reports have documented the abundance of lipids in Mtb-

infected host cells in mice and human (Kondo, Kanai et al. 1970; Kondo and Murohashi 1971; Kondo and Kanai 1976; D'Avila, Melo et al. 2006; Hunter, Jagannath et al. 2007; Peyron, Vaubourgeix et al. 2008; Russell, Cardona et al. 2009). We noted that many of the genes encoding enzymes involved in lipid catabolism and synthesis were markedly upregulated in the transcriptome of the TB granuloma (Table I) and generated an Ingenuity© metabolism plot that was centered around this extensive array of lipid-processing enzymes (Fig 1). The upregulated genes involved in lipid metabolism are interconnected and many of them are unified around the pro-inflammatory cytokine tumor necrosis factor-α (TNF-α), indicating that this response is consistent with a sustained pro-inflammatory insult.

Localization of Proteins Associated with Lipid Synthesis and Sequestration in Human TB Granulomas

We decided to characterize in greater depth the proteins encoded by three highly abundant transcripts relevant to three different aspects of the lipid sequestration and metabolism themes revealed in Figure 1. The selected genes encode ADFP, ACSL1, and PSAP, the precursor of SapC (Table I). These three proteins play different, but key roles in the intracellular processing and sequestration of lipids. ADFP is known to be required for lipid droplet synthesis and remains strongly associated with these droplets following their formation (Robenek, Robenek et al. 2005). Upregulation of ADFP expression increases sequestration of CE, increases synthesis of long-chain fatty acid (LCFA) and TAG, and inhibits catalysis of lipid through the β-oxidation pathway (Larigauderie, Furman et al. 2004;Chang and Chan 2007;Bickel, Tansey et al. 2009). ACSL1 can also lead to the lipid droplet formation through the *de novo* synthesis of LCFAs that are incorporated into TAG (Parkes, Preston et al. 2006;Soupene and Kuypers 2008). Finally, SapC is required for the turnover of sphingolipids, an essential activity to maintain the balance of lipid species in cellular membranes (Harzer, Hiraiwa et al. 2001;Kolter and Sandhoff 2005), which is critical to cells experiencing lipid overload.

To investigate the localization of these proteins within the human TB granulomas, we performed immunohistological analysis on lung tissues excised from TB patients. Tissues from 32 independent Mtb-infected samples (each tissue sample had multiple granulomas) were categorized into four stages: nascent (n=28), caseous (n=16), fibrocaseous (n=66), and resolved granulomas (n=9) (Fig 2). The expression profile of the lipid droplet-associated protein, ADFP, varied markedly through the different stages of granuloma. Nascent granulomas showed weak or minimal staining (Fig 3A), whereas caseous and fibrocaseous granulomas exhibited the highest expression of ADFP (Fig 3B&C). Interestingly, the actual caseum of several granulomas revealed strong staining for ADFP, suggesting that the lipids of the caseum were likely derived from the lipid droplets sequestered within foam cells upon the subsequent death of those cells (Fig 3D). Finally, resolved or calcified granulomas lacked detectable ADFP label (Fig 3E). Type II pneumocytes produce surfactant proteins to reduce surface tension, and the surfactant proteins are cleared or recycled by type II pneumocytes and alveolar macrophages. As a result, those cells possess lipid droplets, and ADFP was readily detected in the normal lung parenchyma (Fig 3F).

The expression pattern of ACSL1 was found to be very similar to that of ADFP. Nascent granulomas had almost no staining, while MGCs occasionally showed very weak staining (Fig 4A). In contrast, the cellular regions subtending the capsules of caseous and fibrocaseous granulomas were robustly stained with the ACSL1 antibody (Fig 4B&C). Similarly to ADFP, resolved granulomas showed no ACSL1 expression, with the exception of a few cells (Fig 4D). ACSL1 is important for normal cell functions; thereby it was detectable in normal lung parenchyma (Fig 4E). SapC expression slightly differed from ADFP and ACSL1 in that it was strongly expressed in macrophages and MGCs even in nascent granulomas (Fig 5A). In caseous and fibrocaseous granulomas, SapC was expressed

along the capsule that contained many macrophages and MGCs (Fig 5B&C). Similarly to ADFP and ACSL1, SapC expression was very weak or not detected in resolved granulomas (Fig 5D). There was no detectable level of SapC expression in normal lung parenchyma (data not shown).

The enhanced expression of these proteins, most notably ADFP, in the macrophage-rich center of the granuloma is indicative of lipid sequestration and foam cell formation. We examined cryosections of human pulmonary TB tissues by staining neutral lipids with Oil Red O and observed lipid-laden foam cells in both respiratory bronchioles and caseous granulomas (Fig S2A–D).

The immunohistological analysis of human TB granulomas enables us to form a more dynamic interpretation of granuloma biology. Both ADFP and ACSL1 are indicative of lipid accumulation through either sequestration or *de novo* synthesis. The paucity of ADFP and ACSL1 expression in nascent granulomas, coupled with their increased expression upon acquisition of the lipid-laden caseum in caseous and fibrocaseous granulomas, suggests a functional linkage.

Analysis of Caseum: Neutral Lipids and Lactosylceramide

The lipid accumulation in Mtb-infected tissues has been reported in studies dating back to early last century (Caldwell 1919; Pagel and Pagel 1925; Kondo, Kanai et al. 1970; Kondo and Murohashi 1971). Moreover, our data indicate that it is a re-alignment in host metabolism that is the most likely explanation for lipid accumulation. To test this hypothesis, we sought to determine the identity of the major lipid species present in the caseum from human pulmonary TB granulomas.

We extracted total lipids from the caseum of caseous or fibrocaseous human pulmonary TB granulomas and from uninvolved lung parenchyma and analyzed them by thin-layer chromatography (TLC). There were noticeable differences in lipid profiles; the caseum had markedly increased amounts of lipids that co-migrated with the CE, CHO, and TAG standards, when compared to lipids isolated from normal lung tissues (Fig 6A). The identities of CE, CHO, and TAG were confirmed by mass spectrometric analysis. Electron impact gas chromatography/mass spectrometry (EI-MS) and total ion current (TIC) chromatogram generated a peak at 12.23 min and an EI mass spectrum that confirmed the presence of CHO (Fig S3A&B). The tandem mass spectrum contained the major $[M + Na]^+$ ions at *m/z* 671.5 and *m/z* 673.8, corresponding to CE (Fig S3C). The dominating $[M+NH_4]^+$ ions were at *m/z* 876.8 corresponding to TAG possessing a total of C_{52} with the presence of 2 total unsaturated bonds situated on the fatty acyl chains (52:2) (Fig S3D).

In addition to these neutral lipids, we observed lipids near the origin that migrated similarly to glycosphingolipids (Fig 6B). Among glycosphingolipids, we detected a unique double band that was identified as LacCer, and ESI-MS analysis revealed $[M + Na]^+$ ions at *m/z* 884.6 and *m/z* 994.8, corresponding to d18:1/16:0-LacCer and d18:1/24.1-LacCer, respectively (Fig S3E).

These data support the hypothesis that there is a functional correlation between the major lipid species in the caseum and the upregulated transcripts and proteins (Fig 1). Foamy macrophages acquire much of their lipids from low-density lipoproteins (LDL), which contains CHO, TAG and glycosphingolipids. The CHO becomes esterified to CE during incorporation into lipid droplets, which are formed through the activity of ADFP. Therefore the presence of CE implicates passage through a macrophage prior to delivery to the caseum.

Mtb-Infected Macrophages Exhibit Upregulation of Lipid Synthesis and Sequestration Pathways

It has been reported previously that Mtb infection induces lipid droplet formation *in vitro* (Kondo and Kanai 1976; Peyron, Vaubourgeix et al. 2008). To determine if this process was associated with increased expression of *ADFP*, *ACSL1*, and *PSAP* (SapC), we infected murine bone marrow-derived macrophages (BMMϕ) and human PBMC-derived macrophages with Mtb. Quantitative real-time RT-PCR (Table II) analysis revealed increased expression of *ADFP*, *ACSL1*, and *PSAP* (SapC) in infected-macrophages. Mtb-infected cells demonstrated lipid droplet formation concomitant with the expression of ADFP, ACSL1, and SapC, revealed by confocal microscopy (Fig 7A–F). The upregulation of these genes was modest in the human PBMC-derived macrophages, however we observed lipid droplet formation even in uninfected human cells (Fig 7G) suggesting that they were already pre-disposed to accumulate lipids.

TDM, a Strong Inducer of Foam Cells in Mice

Recently it was reported that mycolic acids from the cell wall of Mtb were strong inducers of foamy macrophage formation *in vitro* (Korf, Stoltz et al. 2005; Peyron, Vaubourgeix et al. 2008). We had shown previously that Mtb cell wall lipids are released in copious amounts and traffic out of infected macrophages (Beatty, Rhoades et al. 2000; Beatty, Ullrich et al. 2001). We had also demonstrated that amongst these lipids, TDM was the most potent inducer of a granulomatous response and would be an ideal candidate for triggering the pathological response at the infection site (Geisel, Sakamoto et al. 2005; Hunter, Olsen et al. 2006a; Hunter, Olsen et al. 2006b).

To determine whether or not this granulomatous response was accompanied by lipid sequestration, we used the granuloma model we had developed previously (Geisel, Sakamoto et al. 2005; Rhoades, Geisel et al. 2005). Polystyrene beads coated with TDM from Mtb were suspended in Matrigel and inoculated into mice subcutaneously. Murine cells invade the matrix and remodel the site under the influence of the bacterial lipid. Histology of the tissue site revealed an abundance of Adfp-expressing foam cells clustering around the inoculated beads (Fig 8A&B). Cryosections of TDM-induced granuloma also showed an abundance of lipid droplets in foam cells (Fig 8C). Control lipid phosphatidylglycerol (PG)-coated beads recruited very few cells and did not induce foam cell formation (Fig 8D&E). Acsl1 was also detectable in the cells recruited to the TDM-induced granuloma; however, we did not observe detectable levels of SapC expression (data not shown). These data indicate, not surprisingly, that the Mtb lipid TDM is capable of inducing some, but not all, of the features found in the human TB granuloma.

DISCUSSION

The human TB granuloma is a complex structure that has evolved to enable both the host and the pathogen to survive and replicate. However, unlike many chronic infectious agents, Mtb actually promotes the development of a robust, systemic immune response, which it subverts at the localized tissue-level to facilitate its prolonged survival, and, ultimately facilitate its transmission (Russell 2007). The TB granuloma plays a pivotal role in tuberculosis; yet, our knowledge of what determines containment versus active disease is superficial.

In the present study, we sought to elucidate tissue changes that accompany granuloma progression through LCM and microarray analysis of caseous granulomas from human TB patients. Because of the caveats associated with the use of uninfected lung tissue as a control, we generated both hierarchical and comparative lists of transcript abundance; the

overall transcriptional profiles from both methods were strikingly similar. One of the interesting themes to emerge from the microarray data was the apparent re-alignment of lipid metabolism. We chose to focus on the proteins ADFP, ACSL1 and SapC as three key representatives of the lipid-modulating pathways that are impacted by the proinflammatory cytokine TNF-α (Fig 1). ADFP is a member of PAT (perilipin, ADRP, and tail-interacting protein of 47 kDa) domain proteins and is present on the surface and the core of intracellular lipid droplets formed in foam cells. Its mRNA level is increased by excess LCFAs, fasting, modified LDL, peroxisome proliferator-activated receptor (PPAR) agonists, or transcription factors that play a role in lipid homeostasis (Gao and Serrero 1999;Wang, Reape et al. 1999;Larigauderie, Furman et al. 2004;Wei, Taniguchi et al. 2005;Dalen, Ulven et al. 2006;Edvardsson, Ljungberg et al. 2006). In the current study, ADFP was detected in the cells subtending the caseum in caseous and fibrocaseous human pulmonary TB granulomas. ADFP was also observed in newly caseating granulomas, mingled with nuclear debris, implying that the protein was associated with lipid droplets that were released by cells undergoing necrotic or apoptotic death (Fig 3D). ACSL1 and SapC were also strongly expressed in caseous and fibrocaseous human pulmonary TB granulomas. ACSL1 mediates the formation of fatty acyl-CoA esters from fatty acids (preferably chain length of 12 to 20 carbons), which is a key step for lipid biosynthesis and fatty acid degradation, and is also found associated with lipid droplets (Soupene and Kuypers 2008). SapC aids the degradation of glycosphingolipids into ceramide, and sphingosine in acidic compartments, which is critical in maintaining the turn-over of cellular components (Qi, Leonova et al. 1994;Hannun and Obeid 1995;Schuette, Pierstorff et al. 2001;Kolter and Sandhoff 2005). In addition to glycosphingolipid metabolism, SapC is also known to transfer mycobacterial lipid antigen from intralysosomal membrane to CD1b, thereby activating the antigen specific T cells (Winau, Schwierzeck et al. 2004). Our hypothesis that the TB granuloma undergoes a shift in lipid metabolism and accumulates host-derived lipids was supported further by the analysis of the lipid constituents of the caseous material isolated from human pulmonary TB granulomas. Compared to normal lung tissues, the caseum samples were enriched for CE, CHO, TAG, and LacCer (Fig 6A&B). This profile of lipid enrichment is most consistent with the lipids coming from the lipid droplets formed in macrophages that have acquired their lipids from LDL.

The TB literature is rich with reports of lipid accumulation in Mtb infections such as lipid-laden foam cells in human TB lung tissues (Pagel and Pagel 1925; Hunter, Olsen et al. 2006b; Hunter, Jagannath et al. 2007), the accumulation of CE in Mtb infected murine lungs during persistent infection (Kondo, Kanai et al. 1970; Kondo and Murohashi 1971), and the development of lipid droplets in murine or human macrophages infected with virulent Mtb or BCG (Kondo and Kanai 1976; D'Avila, Melo et al. 2006; D'Avila, Roque et al. 2008; Peyron, Vaubourgeix et al. 2008). Lipid droplets are attracting increased attention as dynamic organelles that participate in numerous biological functions linked to metabolic syndromes and diseases including atherosclerosis, diabetes, obesity, heart attack, sepsis, Chagas' disease, and AIDS (Murphy 2001; Desruisseaux, Nagajyothi et al. 2007; Ducharme and Bickel 2008; Bozza, Magalhaes et al. 2009). The data presented in this study provide a new hypothesis for the alterations in tissue physiology that accompany the progression of the human TB granuloma to caseation.

CHO has long been linked to TB; however, data on role(s) of the sterol in disease progression or control are contradictory. The administration of CHO-rich diets to TB patients reduced the number of bacilli in the sputum (Taylor and Bamgboye 1979; Kozarevic, McGee et al. 1981; Perez-Guzman, Vargas et al. 2005; Deniz, Gumus et al. 2007). However, hypercholesterolemic mice through deletion of *ApoE* showed increased Mtb growth and exacerbated lung pathology (Martens, Arikan et al. 2008). This is consistent with the observations of Pandey (Pandey and Sassetti 2008) that CHO supports the growth

of persistent Mtb, and the findings in this current study that the local tissue response to Mtb infection is tightly associated with lipid accumulation. Garton *et al*. reported that Mtb bacilli isolated from sputum samples had TAG-rich intracellular lipophilic inclusions (ILIs) (Garton, Christensen et al. 2002; Garton, Waddell et al. 2008). Prokaryotes have the ability to accumulate lipids (Alvarez and Steinbuchel 2002; Waltermann, Hinz et al. 2005), and Mtb is known to synthesize and accumulate TAG under stress, e.g. starvation and hypoxia (Daniel, Deb et al. 2004; Sirakova, Dubey et al. 2006; Deb, Lee et al. 2009), and encode enzymes to utilize the TAG (Deb, Daniel et al. 2006; Mishra, de Chastellier et al. 2008). Therefore, the accumulated CHO and TAG in caseum of human granulomas may represent a convenient carbon source for either intracellular or extracellular bacilli on the cavitary surface of TB granulomas. LacCer is an extremely interesting glycosphingolipid to be found in abundance in the caseum with respect to its biological properties in glycosphingolipid metabolism. It is normally present in trace amounts in mammalian cells because it is an intermediate in the glycosphingolipids metabolism (Kolter and Sandhoff 2005; Kolter and Sandhoff 2006). Its accumulation in cells could be the result of either increased ceramide synthase activity or the increased catabolism of complex ceramides (Chatterjee and Pandey 2008). The upregulation of SapC within the granulomas favors the explanation that the tissue may be experiencing LacCer excess and is trying to degrade the lipid through promoting the activities of β-galactosidase and β-glucosidase, the expression of which were upregulated 20 fold and 32 fold respectively in the TB granuloma (Table I). In addition to the endogenous generation of LacCer, treatment of cells with LacCer is known to reduce CHO efflux and enhances foam cell formation (Glaros, Kim et al. 2005). Further studies need to be done to fully verify the origin(s) of CE, CHO, TAG, and LacCer that accumulate in human TB granuloma caseum.

Lesions of *Mycobacterium leprae*-infected lepromatous leprosy patients show significant accumulation of oxidized phospholipids (Cruz, Watson et al. 2008). Intriguingly, several of the genes reported as upregulated in our study overlap with those observed in lepromatous leprosy lesions, including *PSAP* and *ADFP* (Cruz, Watson et al. 2008). Another study also demonstrated the accumulation of neutral lipids including CE and the localization of ADFP protein in leprosy lesions (Mattos, D'Avila et al. 2010). These data indicate that there are many parallels to the metabolic reprogramming induced by both Mtb and *M. leprae*. The point at which the two infection sites diverge could hinge on the formation of the fibrous capsule in the TB granuloma, which may focus and constrain the inflammatory response leading to the accumulation of the sequestered lipids as caseum. This pathology is unique to Mtb infection and precedes the liquefaction and cavitation of the lesion. In mice, this late-stage pathology was absent from experimental Mtb infections, which has led many researchers to be concerned about the validity of the mouse as an experimental model. Recently, however, Hunter and colleagues reported caseum formation in reactivation disease in antibiotic-treated mice (Hunter, Jagannath et al. 2007). Significantly, these murine caseous lesions exhibited a highly developed fibrous capsule comparable to that observed in fibrocaseous human granulomas.

We also have shown that Mtb infection of macrophages *in vitro* induces foam cell formation, and that inoculation of beads coated with the bacterial cell wall lipid TDM into mice caused the clustering of Adfp-expressing foam cells around the particles. These data argue strongly that lipid sequestration is a pathogen-induced response. We have demonstrated previously that mycobacterial cell wall lipid-containing vesicles, which contain TDM, are released from infected macrophages and spread the influence of the bacterium to neighboring cells (Beatty, Rhoades et al. 2000; Russell, Mwandumba et al. 2002; Rhoades, Hsu et al. 2003). TDM activates macrophages by signaling through TLR2, which forms a functional complex with the scavenger receptor MARCO to bind the mycobacterial lipid (Bowdish, Sakamoto et al. 2009). This amplification of the response

from infected cells to uninfected bystander cells could explain the extreme tissue reaction observed in human TB granulomas when the bacterial density is known to be relatively low (data not shown) (Ulrichs, Lefmann et al. 2005).

The current study provides a new framework for appreciating the physiological responses to Mtb infection that accompany the progression of TB granulomas to caseation and cavitation, and ultimately disease transmission. We hypothesize that bacterial components, such as TDM, stimulate the host's innate immune response to enhance synthesis and/or sequestration of host lipids in the form of lipid droplets. The foamy macrophages accumulate in the macrophage-rich center of the granuloma, where ultimately they die through either apoptosis or necrosis. This leads to the buildup of lipids as caseum, and, finally to cavitation and release of infectious Mtb bacilli (Fig 9). Our data argue that the development of novel therapeutics should encompass manipulation of the host's local response and not be restricted to antimicrobials. Targeting fatty acid metabolism, lipid deposition, and lipid-mediated cell death in host cells are unlikely to impact on bacterial growth directly, however, they may influence the tissue response to Mtb infection and thereby modulate TB disease progression.

METHODS

Human Subjects

Human subjects were included in this study according to protocols approved by Institutional Review Boards at University of Cape Town, South Africa, the Public Health Research Institute, Newark, NJ, and Cornell University, Ithaca, NY. Informed consent was obtained from all of patients.

Animals

C57BL/6J mice were obtained from the Jackson Laboratory and housed under specific-pathogen-free conditions. All experiments were approved by Cornell University Institutional Animal Care and Use Committee.

Tissue Specimens

Human TB lung tissues were surgically excised from TB patients who had extensive lung cavitation and tissue degeneration, that showed little response to the antibiotics. Snap-frozen tissues were transported from Groote Schuur Hospital of Cape Town to our biosafety level-3 (BL3) laboratory. Frozen samples were embedded in O.C.T. compound (Tissue-Tek®), cut into 10 μm-thick sections at −25°C on a Cryocut 1800 cryostat (Leica Microsystems) and attached onto PET-membrane frame slides (Leica Microsystems) for laser capture microdissection or Superfrost Plus Micro slides (Erie Scientific) for histological examination.

Histology of Human Tissues

Human TB lung tissues embedded in paraffin were cut at 3 μm thickness and stained with hematoxylin & eosin (H&E) for histological examination. Cryosections of human TB lung tissues were fixed in 4% paraformaldehyde in PBS for 30 min and stained with H&E, and then paired to PET-membrane slides prepared for LCM. For the detection of neutral lipids, fixed cryosections were stained with Oil Red O (Alfa Aesar) and counterstained with hematoxylin.

Laser Capture Microdissection

Tissue sections mounted onto PET-membrane slides were fixed in graded ethanol (70%, 75%, 96%, and 100%) containing 0.5% sodium azide for 30 sec per each step. Slides were air dried briefly, and areas of interest were dissected by using Leica AS LMD system (Leica Microsystems).

Microarray

Total RNA was isolated from LCM-derived materials using PicoPure™ RNA Isolation Kit (Arcturus) and treated with DNase using TURBO DNA-*free*™ (Ambion). Purity, quality, and quantity of RNA were assessed by the Agilent NanoChip Bioanalyzer assay, spectrophotometer, and reverse-transcription PCR (RT-PCR) of β-actin (234 bp), glyceraldehyde-3-phosphate dehydrogenase (GAPDH, 189 bp), 18S rRNA (236 bp), and ubiquitin (198 bp). To obtain sufficient quantities of RNA for microarray, two-rounds of linear amplification of RNA were conducted using RiboAmp HS™ Amplification Kit (Arcturus) and BioArray High Yield™ RNA Transcript Labeling Kit (T7) (Enzo Life Sciences, Inc.). Biotinylated, amplified antisense RNA was fragmented and hybridized onto GeneChip® Human X3P Array (Affymetrix), and the chip was scanned by GeneArray 300 scanner (Affymetrix). We performed three independent arrays on one LCM-derived granuloma sample, which confirmed the reliability of the technique. Thereafter, two other granulomas were further analyzed by microarray for biological replicates.

Microarray Data Analysis

For the generation of a hierarchical list of absolute gene expressions in caseous human TB lung granulomas, raw CEL files were analyzed at the probe level using R and Bioconductor. Only perfect match (PM) probes were included in the estimation for expression level of probe sets. Raw PM intensities from each array were subjected to local background correction using MAS5 method, $\log_2$-transformed and median-centered. Informative PM probes from each probe set were selected as having the highest mean across all arrays. In this study, the mean signal of top 5 informative PM probes of each probe set was used to represent its expression level. For a list of genes differentially expressed between caseous human pulmonary TB granulomas and normal lung parenchyma, raw CHP files were summarized by MAS5 method and scaled to median of all samples, and the baseline was transformed to the median of all samples, by using GeneSpring GX 10.0.2 program (Agilent Technologies). The networks were generated through the use of Ingenuity Pathway Analysis (Ingenuity® Systems, www.ingenuity.com).

Statistical Analysis

The statistical significance of differences in gene expressions between normal human lung tissues and caseous human TB lung granulomas was calculated using an unpaired *t* test with Benjamini-Hochberg correction. Results with a *P* value less than 0.05 were considered significant.

Culture and *in vitro* Infection of Macrophages

Bone marrow cells were isolated from femurs and tibias of 6–8 week-old female C57BL/6 mice and cultured in Dulbecco's Modified Eagle Medium (DMEM, Gibco) supplemented with 20% L-929 cell-conditioned medium, 10% heat-inactivated fetal calf serum (Hyclone), 2 mM L-glutamine (Gibco), 1 mM sodium pyruvate (Gibco), and 100 U/ml penicillin-100 μg/ml streptomycin (Gibco) at 37°C, 5% CO_2, and 90% humidity for five days. BMMΦ were incubated with Mtb H37Rv at a multiplicity of infection 20:1 (bacteria per macrophage) for 2h, washed with PBS and cultured DMEM medium without antibiotics.

Monocytes were isolated from human blood (Zen-Bio Inc.) by gradient separation. Briefly, blood was mixed with an equal volume of PBS, and 25 ml of this mixture was laid over 12ml of Histopaque®-10771 (Sigma, density=1.0771 g/ml). The leukocyte-containing layer was harvested, washed and cultured in DMEM medium as in BMMΦ culture, but without L-929 cell-conditioned medium. Differentiated human PBMC-derived macrophages were incubated with Mtb H37Rv at a MOI 10:1 (bacteria per MΦ) for 2 h, washed with PBS and cultured in DMEM medium without antibiotics.

Quantitative real-time RT-PCR

Infected and uninfected macrophages were lysed with TRIZOL® Reagent (Invitrogen) and homogenized by passing cell lysate through a pipette. The homogenized samples were mixed with 0.2 volume of chloroform per 1 volume of TRIZOL® Reagent, and phases were separated by centrifugation. The RNA-containing aqueous phase was column-purified using RNEasy mini kit (Qiagen). RNA samples were treated with DNase using TURBO DNA-*free*™ (Ambion). The cDNA was synthesized using iScript™ cDNA Synthesis Kit (BIO-RAD) and used for real-time PCR using iTaq™ SYBR® Green Supermix with ROX (BIO-RAD) in 7500 Fast Real-Time PCR System (Applied Biosystems). Each PCR was done in triplicate, and PCR conditions are as follows: initial activation at 95°C for 2 min and 40 cycles of denaturation at 95°C for 30 sec and annealing and extension at 53°C for 45 sec. Forward and reverse primers designed by using Primer3 are shown in Table SIII (Rozen and Skaletsky 2000). The calculated threshold cycle (C_t) value for each gene was normalized to C_t of house-keeping gene 18S rRNA, and then the fold induction of gene of interest between control MΦ and Mtb-infected MΦ was calculated and presented by using the formula, $2^{-\Delta\Delta Ct}$.

Confocal Microscopy of Macrophages

Cells were fixed in 4% paraformaldehyde in PBS for 30 min, washed and blocked with 5% bovine serum albumin (Sigma), 1.5% glycine (VWR International), and 0.1% saponin in PBS at room temperature for 1h. Cells were incubated with guinea pig polyclonal antibody against murine Adfp or mouse monoclonal antibody against human ADFP (1:100, RDI division of Fitzgerald Industries Intl.), rabbit polyclonal antibody against human ACSL1 (1:200, GenWay Biotech), or rabbit polyclonal antibody against human SapC (1:50, Santa Cruz Biotechnology) at 37°C for 1h. After washing with PBS, cells were incubated with Texas Red®-conjugated antibodies against guinea pig, mouse, or rabbit (1:250, Jackson ImmunoResearch) and BODIPY® 493/503 (1 μg/ml, Invitrogen) for lipid droplets, at room temperature for 1h. After wash with PBS, the nuclei were stained with 5 μg/ml of bisbenzimide (Sigma) prior to mounting the cells in ProLong Gold Antifade Reagent (Molecular Probes®). Cells without primary antibodies were included as a control. Cells were examined by Leica TCS SP5 confocal laser scanning microscope (Leica Microsystems) using a 63× oil immersion lens.

Immunofluorescence Microscopy of Human TB Lung Tissues

Paraffin-embedded sections of 3 μm thickness were heat-fixed, deparaffinized and rehydrated. Epitopes were heat-retrieved in a pressure cooker with 1 mM EDTA buffer pH 8.0, and tissue sections were blocked with 0.2% gelatin in PBS with 0.05% Tween-20 (PBS-T) at room temperature for 1 h. Primary antibodies, mouse monoclonal antibody against human ADFP (1:100, RDI division of Fitzgerald Industrial Intl.), rabbit polyclonal antibody against human ACSL1 (1:150, GenWay Biotech), or rabbit polyclonal antibody against human saposin C (1:50, Santa Cruz Biotechnology) were applied to tissue sections at 37°C for 1h. After washing h BS-T, sections were incubated with 1% Sudan Black B (Sigma) in 7% ethanol at room temperature for 10 min. Sections were washed with PBS-T and incubated with andCy3™-goat antibody against mouse or rabbit (1:250, Jackson

ImmunoResearch) at room temperature for 45 min. After PBS-T wash, nuclei were stained with 1 μg/ml of DAPI (Invitrogen) and the tissue sections were mounted in ProLong Gold Antifade Reagent, prior to examination. Images were captured by Zeiss Axioskop 40 epifluorescence microscope with AxioVision 4.3 software (Carl Zeiss MicroImaging). Further image analysis was done by AxioVision LE software (Carl Zeiss MicroImaging).

Lipid Analysis

Frozen human TB lung tissues or normal lung tissues were thawed, and caseum or normal tissue segments were isolated and transferred into glass vials (Wheaton Science) and then mixed with chloroform:methanol (2:1, v/v). After sonication at 50°C for 1h, the extracts were filtered through 0.2 μm-pore size PTFE membrane (GD/X® syringe filter, Whatman) and dried down using nitrogen. TLC plates (aluminum-backed Silica gel 60 plates, EMD) were pre-run in chloroform:methanol (90:10, v/v) to remove contaminants from silica gel followed by heat-activation at 110°C for 30 min. Total lipids were developed either in a dual solvent system of chloroform:methanol:water (65:25:4, v/v/v) and petroleum ether:ethyl ether:acetic acid (70:30:2, v/v/v), or in a single solvent system of chloroform:methanol:water (65:25:4, v/v/v). Plates were sprayed with 50% sulfuric acid in ethanol and charred. The lipid standards used were cholesteryl oleate, TAG, cardiolipin, and phosphatidylcholine (Sigma), cholesterol (MP Biomedicals), sphingomyelin (Avanti Polar Lipids), and neutral glycosphingolipid qualmix (Matreya). Caseous and fibrocaseous granuloma samples were derived from seven independent tissue samples, and normal lung tissues were from the unaffected lung area of seven independent tissue samples.

Mass-Spectrometry

Structural analysis of lipids including SM, LacCer, CE, and TAG were carried out by a Finnigan TSQ-7000 triple stage quadrupole mass spectrometer (Thermo Electron Corporation, CA) equipped with a Finnigan ESI source and controlled by Finnigan ICIS software operated on a DEC alpha workstation. Lipid extract dissolved in methanol/chloroform (2:1, v/v) were continuously infused into the ESI source with a Harvard syringe pump at a flow rate of 1μL/min. The skimmer was at ground potential, and the electrospray needle was at 4.5 kV. The heated capillary temperature was 250°C. The collisionally activated dissociation (CAD) tandem mass spectra were obtained under collision energy from 30 to 45 eV, and argon (2.3 mTorr) was used as target gas. The product ion spectra were acquired in the profile mode at the scan rate of one scan per 3 sec.

Structural characterization of CH was conducted by Agilent 5973 MSD GC/MS system operated by ChemStation software. Lipid extract in methanol/chloroform (2:1, v/v) was injected into a Hewett-Packard 6890 GC in a splitless mode and analyzed with a 15 m DB-1701 column (0.25 mm i.d, 0.25 μm film thickness; J & W Scientific). The initial temperature of GC was set at 100°C for 1 min, increased to 220°C at a rate of 50°C/min, then to 290°C at a rate of 10°C/min and maintained at 290°C for another 10 min. The temperatures of the injector, transfer line of the GC column and of the ion-source were set at 280°C, 280°C and 230°C, respectively. The full scan mass spectra (50 to 500 Da) were acquired at a rate of 1 scan/0.25 Sec.

In vivo Murine Granuloma Model

Mycobacterial lipid-bearing beads were prepared as described previously, with slight modifications (Geisel, Sakamoto et al. 2005; Rhoades, Geisel et al. 2005). Briefly, 9.25×10^3 of 80 μm polystyrene microspheres (Duke Scientific) were coated with 15 μg of Mtb-derived trehalose dimycolate (TDM, Sigma) or control lipid phosphatidylglycerol (PG, Sigma) by alternative cycles of vortexing and sonication. The TDM- or PG- coated beads were resuspended in 300 μl of ice-cold growth-factor reduced Matrigel (BD). The mixture

was injected sub-dermally into the skin fold at the scruff of the neck. Granulomas were excised at 6 days post-inoculation. Three or four mice were used for the injection of TDM- or PG-Matrigel mixture. The experiment was repeated more than three times.

Histology and Immunohistology of Murine Granulomas

Granulomas were fixed in 4% paraformaldehyde in PBS at 4°C for over 24 hours and transferred to 70% ethanol. Sections were stained with hematoxylin & eosin for histological examination. For immunostaining, paraffin-embedded sections were heat-fixed, deparaffinized and rehydrated. Epitopes were heat-retrieved in 1 mM EDTA buffer pH 8.0, and tissue sections were blocked with 5% BSA in PBS at room temperature for 1 hour. Guinea pig polyclonal antibody against murine Adfp (1:200, RDI division of Fitzgerald Industrial Intl.) or rabbit polyclonal antibody against human ACSL1 (1:150, GenWay Biotech) was applied to sections at 37°C for 1 hour. After washing with PBS three times, sections were incubated with 1% Sudan Black B (Sigma) in 70% ethanol at room temperature for 10 min. Sections were washed with PBS three times and incubated with Texas Red®-donkey antibody against guinea pig IgG (H+L) (1:250, Jackson ImmunoResearch) or Texas Red®-goat antibody against rabbit IgG (H+L) (1:250, Jackson ImmunoResearch) at room temperature for 45 min. After three washes with PBS, nuclei were stained with 5 μg/ml of bisbenzimide (Sigma) in PBS at room temperature for 5 min. After thorough wash with PBS, sections were mounted in ProLong Gold Antifade Reagent (Molecular Probes®). Sections without primary antibody were included as a negative control. Images were captured by Zeiss Axio Imager with AxioVision LE software (Carl Zeiss MicroImaging). Cryosections were cut at 10 μm thickness and fixed in 4% paraformaldehyde in PBS for 20 min. The sections were stained with Nile Red (1 μg/ml, Sigma) for neutral lipids and with bisbenzimide for nuclei. Mounted sections were visualized by Zeiss Axio Imager with AxioVision LE software (Carl Zeiss MicroImaging).

Supplementary Material

Refer to Web version on PubMed Central for supplementary material.

Acknowledgments

This work was supported by funds from the National Institutes of Health HL055936 to DGR and AI054338 to GK.

References

Actor JK, Olsen M, et al. Dysregulated response to mycobacterial cord factor trehalose-6,6′-dimycolate in CD1D−/− mice. J Interferon Cytokine Res 2001;21(12):1089–1096. [PubMed: 11798467]

Alvarez HM, Steinbuchel A. Triacylglycerols in prokaryotic microorganisms. Appl Microbiol Biotechnol 2002;60(4):367–376. [PubMed: 12466875]

Beatty WL, Rhoades ER, et al. Trafficking and release of mycobacterial lipids from infected macrophages. Traffic 2000;1(3):235–247. [PubMed: 11208107]

Beatty WL, Ullrich HJ, et al. Mycobacterial surface moieties are released from infected macrophages by a constitutive exocytic event. Eur J Cell Biol 2001;80(1):31–40. [PubMed: 11211933]

Bickel PE, Tansey JT, et al. PAT proteins, an ancient family of lipid droplet proteins that regulate cellular lipid stores. Biochim Biophys Acta 2009;1791(6):419–440. [PubMed: 19375517]

Bild AH, Yao G, et al. Oncogenic pathway signatures in human cancers as a guide to targeted therapies. Nature 2006;439(7074):353–357. [PubMed: 16273092]

Bowdish DM, Sakamoto K, et al. MARCO, TLR2, and CD14 are required for macrophage cytokine responses to mycobacterial trehalose dimycolate and Mycobacterium tuberculosis. PLoS Pathog 2009;5(6):e1000474. [PubMed: 19521507]

Bozza PT, Magalhaes KG, et al. Leukocyte lipid bodies - Biogenesis and functions in inflammation. Biochim Biophys Acta 2009;1791(6):540–551. [PubMed: 19416659]

Caldwell G. Chemical Changes in Tuberculous Tissues. The Journal of Infectious Diseases 1919;24:81–113.

Chang BH, Chan L. Regulation of Triglyceride Metabolism. III. Emerging role of lipid droplet protein ADFP in health and disease. Am J Physiol Gastrointest Liver Physiol 2007;292(6):G1465–1468. [PubMed: 17194897]

Chatterjee S, Pandey A. The Yin and Yang of lactosylceramide metabolism: implications in cell function. Biochim Biophys Acta 2008;1780(3):370–382. [PubMed: 18077097]

Chatterjee SB, Dey S, et al. Accumulation of glycosphingolipids in human atherosclerotic plaque and unaffected aorta tissues. Glycobiology 1997;7(1):57–65. [PubMed: 9061365]

Cruz D, Watson AD, et al. Host-derived oxidized phospholipids and HDL regulate innate immunity in human leprosy. J Clin Invest 2008;118(8):2917–2928. [PubMed: 18636118]

D'Avila H, Melo RC, et al. Mycobacterium bovis bacillus Calmette-Guerin induces TLR2-mediated formation of lipid bodies: intracellular domains for eicosanoid synthesis in vivo. J Immunol 2006;176(5):3087–3097. [PubMed: 16493068]

D'Avila H, Roque NR, et al. Neutrophils recruited to the site of Mycobacterium bovis BCG infection undergo apoptosis and modulate lipid body biogenesis and prostaglandin E production by macrophages. Cell Microbiol 2008;10(12):2589–2604. [PubMed: 18771558]

Dalen KT, Ulven SM, et al. PPARalpha activators and fasting induce the expression of adipose differentiation-related protein in liver. J Lipid Res 2006;47(5):931–943. [PubMed: 16489205]

Daniel J, Deb C, et al. Induction of a novel class of diacylglycerol acyltransferases and triacylglycerol accumulation in Mycobacterium tuberculosis as it goes into a dormancy-like state in culture. J Bacteriol 2004;186(15):5017–5030. [PubMed: 15262939]

Dannenberg AM Jr. Roles of cytotoxic delayed-type hypersensitivity and macrophage-activating cell-mediated immunity in the pathogenesis of tuberculosis. Immunobiology 1994;191(4–5):461–473. [PubMed: 7713560]

Dannenberg AM Jr, Sugimoto M. Liquefaction of caseous foci in tuberculosis. Am Rev Respir Dis 1976;113(3):257–259. [PubMed: 816235]

Deb C, Daniel J, et al. A novel lipase belonging to the hormone-sensitive lipase family induced under starvation to utilize stored triacylglycerol in Mycobacterium tuberculosis. J Biol Chem 2006;281(7):3866–3875. [PubMed: 16354661]

Deb C, Lee CM, et al. A novel in vitro multiple-stress dormancy model for Mycobacterium tuberculosis generates a lipid-loaded, drug-tolerant, dormant pathogen. PLoS One 2009;4(6):e6077. [PubMed: 19562030]

Deniz O, Gumus S, et al. Serum total cholesterol, HDL-C and LDL-C concentrations significantly correlate with the radiological extent of disease and the degree of smear positivity in patients with pulmonary tuberculosis. Clin Biochem 2007;40(3–4):162–166. [PubMed: 17217941]

Desruisseaux, Nagajyothi MS, et al. Adipocyte, adipose tissue, and infectious disease. Infect Immun 2007;75(3):1066–1078. [PubMed: 17118983]

Ducharme NA, Bickel PE. Lipid droplets in lipogenesis and lipolysis. Endocrinology 2008;149(3): 942–949. [PubMed: 18202123]

Dye C, Bassili A, et al. Measuring tuberculosis burden, trends, and the impact of control programmes. Lancet Infect Dis 2008;8(4):233–243. [PubMed: 18201929]

Edvardsson U, Ljungberg A, et al. PPARalpha activation increases triglyceride mass and adipose differentiation-related protein in hepatocytes. J Lipid Res 2006;47(2):329–340. [PubMed: 16282640]

Gao J, Serrero G. Adipose differentiation related protein (ADRP) expressed in transfected COS-7 cells selectively stimulates long chain fatty acid uptake. J Biol Chem 1999;274(24):16825–16830. [PubMed: 10358026]

Garner B, Mellor HR, et al. Modulation of THP-1 macrophage and cholesterol-loaded foam cell apolipoprotein E levels by glycosphingolipids. Biochem Biophys Res Commun 2002;290(5): 1361–1367. [PubMed: 11820771]

Garton NJ, Christensen H, et al. Intracellular lipophilic inclusions of mycobacteria in vitro and in sputum. Microbiology 2002;148(Pt 10):2951–2958. [PubMed: 12368428]

Garton NJ, Waddell SJ, et al. Cytological and transcript analyses reveal fat and lazy persister-like bacilli in tuberculous sputum. PLoS Med 2008;5(4):e75. [PubMed: 18384229]

Geisel RE, Sakamoto K, et al. In vivo activity of released cell wall lipids of Mycobacterium bovis bacillus Calmette-Guerin is due principally to trehalose mycolates. J Immunol 2005;174(8):5007–5015. [PubMed: 15814731]

Glaros EN, Kim WS, et al. Glycosphingolipid accumulation inhibits cholesterol efflux via the ABCA1/apolipoprotein A-I pathway: 1-phenyl-2-decanoylamino-3-morpholino-1-propanol is a novel cholesterol efflux accelerator. J Biol Chem 2005;280(26):24515–24523. [PubMed: 15890646]

Grassi M, Bocchino M, et al. Transcriptional profile of the immune response in the lungs of patients with active tuberculosis. Clin Immunol 2006;121(1):100–107. [PubMed: 16905363]

Hannun YA, Obeid LM. Ceramide: an intracellular signal for apoptosis. Trends Biochem Sci 1995;20(2):73–77. [PubMed: 7701566]

Harzer K, Hiraiwa M, et al. Saposins (sap) A and C activate the degradation of galactosylsphingosine. FEBS Lett 2001;508(1):107–110. [PubMed: 11707278]

Hunter RL, Jagannath C, et al. Pathology of postprimary tuberculosis in humans and mice: contradiction of long-held beliefs. Tuberculosis (Edinb) 2007;87(4):267–278. [PubMed: 17369095]

Hunter RL, Olsen M, et al. Trehalose 6,6′-dimycolate and lipid in the pathogenesis of caseating granulomas of tuberculosis in mice. Am J Pathol 2006a;168(4):1249–1261. [PubMed: 16565499]

Hunter RL, Olsen MR, et al. Multiple roles of cord factor in the pathogenesis of primary, secondary, and cavitary tuberculosis, including a revised description of the pathology of secondary disease. Ann Clin Lab Sci 2006b;36(4):371–386. [PubMed: 17127724]

Karakousis PC, Yoshimatsu T, et al. Dormancy phenotype displayed by extracellular Mycobacterium tuberculosis within artificial granulomas in mice. J Exp Med 2004;200(5):647–657. [PubMed: 15353557]

Kim DK, Park GM, et al. Microarray analysis of gene expression associated with extrapulmonary dissemination of tuberculosis. Respirology 2006;11(5):557–565. [PubMed: 16916327]

Kolter T, Sandhoff K. Principles of lysosomal membrane digestion: stimulation of sphingolipid degradation by sphingolipid activator proteins and anionic lysosomal lipids. Annu Rev Cell Dev Biol 2005;21:81–103. [PubMed: 16212488]

Kolter T, Sandhoff K. Sphingolipid metabolism diseases. Biochim Biophys Acta 2006;1758(12):2057–2079. [PubMed: 16854371]

Kondo E, Kanai K. Accumulation of cholesterol esters in macrophages incubated with mycobacteria in vitro. Jpn J Med Sci Biol 1976;29(3):123–137. [PubMed: 824482]

Kondo E, Kanai K, et al. Analysis of host-originated lipids associated with “in vivo grown tubercle bacilli”. Jpn J Med Sci Biol 1970;23(5):315–326. [PubMed: 4925915]

Kondo E, Murohashi T. Esterification of tissue cholesterol with fatty acids in the lungs of tuberculous mice. Jpn J Med Sci Biol 1971;24(6):345–356. [PubMed: 4946849]

Korf J, Stoltz A, et al. The Mycobacterium tuberculosis cell wall component mycolic acid elicits pathogen-associated host innate immune responses. Eur J Immunol 2005;35(3):890–900. [PubMed: 15724242]

Kozarevic D, McGee D, et al. Serum cholesterol and mortality: the Yugoslavia Cardiovascular Disease Study. Am J Epidemiol 1981;114(1):21–28. [PubMed: 7246527]

Larigauderie G, Furman C, et al. Adipophilin enhances lipid accumulation and prevents lipid efflux from THP-1 macrophages: potential role in atherogenesis. Arterioscler Thromb Vasc Biol 2004;24(3):504–510. [PubMed: 14707038]

Ma XJ, Dahiya S, et al. Gene expression profiling of the tumor microenvironment during breast cancer progression. Breast Cancer Res 2009;11(1):R7. [PubMed: 19187537]

Martens GW, Arikan MC, et al. Hypercholesterolemia impairs immunity to tuberculosis. Infect Immun 2008;76(8):3464–3472. [PubMed: 18505807]

Mattos KA, D'Avila H, et al. Lipid droplet formation in leprosy: Toll-like receptor-regulated organelles involved in eicosanoid formation and Mycobacterium leprae pathogenesis. J Leukoc Biol 2010;87(3):371–384. [PubMed: 19952355]

Mishra KC, de Chastellier C, et al. Functional role of the PE domain and immunogenicity of the Mycobacterium tuberculosis triacylglycerol hydrolase LipY. Infect Immun 2008;76(1):127–140. [PubMed: 17938218]

Murphy DJ. The biogenesis and functions of lipid bodies in animals, plants and microorganisms. Prog Lipid Res 2001;40(5):325–438. [PubMed: 11470496]

Pagel W, Pagel M. Zur Histochemie der Lungentuberkulose, mit besonderer Berücksichtigung der Fettsubstanzen und Lipoide. Virchows Archiv 1925;256(3):629–640.

Pandey AK, Sassetti CM. Mycobacterial persistence requires the utilization of host cholesterol. Proc Natl Acad Sci U S A 2008;105(11):4376–4380. [PubMed: 18334639]

Parkes HA, Preston E, et al. Overexpression of acyl-CoA synthetase-1 increases lipid deposition in hepatic (HepG2) cells and rodent liver in vivo. Am J Physiol Endocrinol Metab 2006;291(4):E737–744. [PubMed: 16705061]

Perez-Guzman C, Vargas MH, et al. A cholesterol-rich diet accelerates bacteriologic sterilization in pulmonary tuberculosis. Chest 2005;127(2):643–651. [PubMed: 15706008]

Peyron P, Vaubourgeix J, et al. Foamy macrophages from tuberculous patients' granulomas constitute a nutrient-rich reservoir for M. tuberculosis persistence. PLoS Pathog 2008;4(11):e1000204. [PubMed: 19002241]

Puissegur MP, Botanch C, et al. An in vitro dual model of mycobacterial granulomas to investigate the molecular interactions between mycobacteria and human host cells. Cell Microbiol 2004;6(5): 423–433. [PubMed: 15056213]

Qi X, Leonova T, et al. Functional human saposins expressed in Escherichia coli. Evidence for binding and activation properties of saposins C with acid beta-glucosidase. J Biol Chem 1994;269(24): 16746–16753. [PubMed: 8206997]

Ragno S, Romano M, et al. Changes in gene expression in macrophages infected with Mycobacterium tuberculosis: a combined transcriptomic and proteomic approach. Immunology 2001;104(1):99–108. [PubMed: 11576227]

Rhoades E, Hsu F, et al. Identification and macrophage-activating activity of glycolipids released from intracellular Mycobacterium bovis BCG. Mol Microbiol 2003;48(4):875–888. [PubMed: 12753183]

Rhoades ER, Geisel RE, et al. Cell wall lipids from Mycobacterium bovis BCG are inflammatory when inoculated within a gel matrix: characterization of a new model of the granulomatous response to mycobacterial components. Tuberculosis (Edinb) 2005;85(3):159–176. [PubMed: 15850754]

Robenek H, Robenek MJ, et al. Lipid droplets gain PAT family proteins by interaction with specialized plasma membrane domains. J Biol Chem 2005;280(28):26330–26338. [PubMed: 15897193]

Rozen S, Skaletsky H. Primer3 on the WWW for general users and for biologist programmers. Methods Mol Biol 2000;132:365–386. [PubMed: 10547847]

Russell DG. Who puts the tubercle in tuberculosis? Nat Rev Microbiol 2007;5(1):39–47. [PubMed: 17160001]

Russell DG, Cardona PJ, et al. Foamy macrophages and the progression of the human tuberculosis granuloma. Nat Immunol 2009;10(9):943–948. [PubMed: 19692995]

Russell DG, Mwandumba HC, et al. Mycobacterium and the coat of many lipids. J Cell Biol 2002;158(3):421–426. [PubMed: 12147678]

Schuette CG, Pierstorff B, et al. Sphingolipid activator proteins: proteins with complex functions in lipid degradation and skin biogenesis. Glycobiology 2001;11(6):81R–90R.

Sirakova TD V, Dubey S, et al. Identification of a diacylglycerol acyltransferase gene involved in accumulation of triacylglycerol in Mycobacterium tuberculosis under stress. Microbiology 2006;152(Pt 9):2717–2725. [PubMed: 16946266]

Soupene E, Kuypers FA. Mammalian long-chain acyl-CoA synthetases. Exp Biol Med (Maywood) 2008;233(5):507–521. [PubMed: 18375835]

Taylor GO, Bamgboye AE. Serum cholesterol and diseases in Nigerians. Am J Clin Nutr 1979;32(12): 2540–2545. [PubMed: 506976]

Tuomisto TT, Yla-Herttuala S. What have we learnt about microarray analyses of atherogenesis? Curr Opin Lipidol 2005;16(2):201–205. [PubMed: 15767860]

Ulrichs T, Kaufmann SH. New insights into the function of granulomas in human tuberculosis. J Pathol 2006;208(2):261–269. [PubMed: 16362982]

Ulrichs T, Lefmann M, et al. Modified immunohistological staining allows detection of Ziehl-Neelsen-negative Mycobacterium tuberculosis organisms and their precise localization in human tissue. J Pathol 2005;205(5):633–640. [PubMed: 15776475]

Volpe E, Cappelli G, et al. Gene expression profiling of human macrophages at late time of infection with Mycobacterium tuberculosis. Immunology 2006;118(4):449–460. [PubMed: 16895554]

Waltermann M, Hinz A, et al. Mechanism of lipid-body formation in prokaryotes: how bacteria fatten up. Mol Microbiol 2005;55(3):750–763. [PubMed: 15661001]

Wang X, Reape TJ, et al. Induced expression of adipophilin mRNA in human macrophages stimulated with oxidized low-density lipoprotein and in atherosclerotic lesions. FEBS Lett 1999;462(1–2): 145–150. [PubMed: 10580108]

Wei P, Taniguchi S, et al. Expression of adipose differentiation-related protein (ADRP) is conjointly regulated by PU.1 and AP-1 in macrophages. J Biochem 2005;138(4):399–412. [PubMed: 16272134]

Winau F, Schwierzeck V, et al. Saposin C is required for lipid presentation by human CD1b. Nat Immunol 2004;5(2):169–174. [PubMed: 14716313]

Zhu G, Xiao H, et al. Gene expression in the tuberculous granuloma: analysis by laser capture microdissection and real-time PCR. Cell Microbiol 2003;5(7):445–453. [PubMed: 12814435]

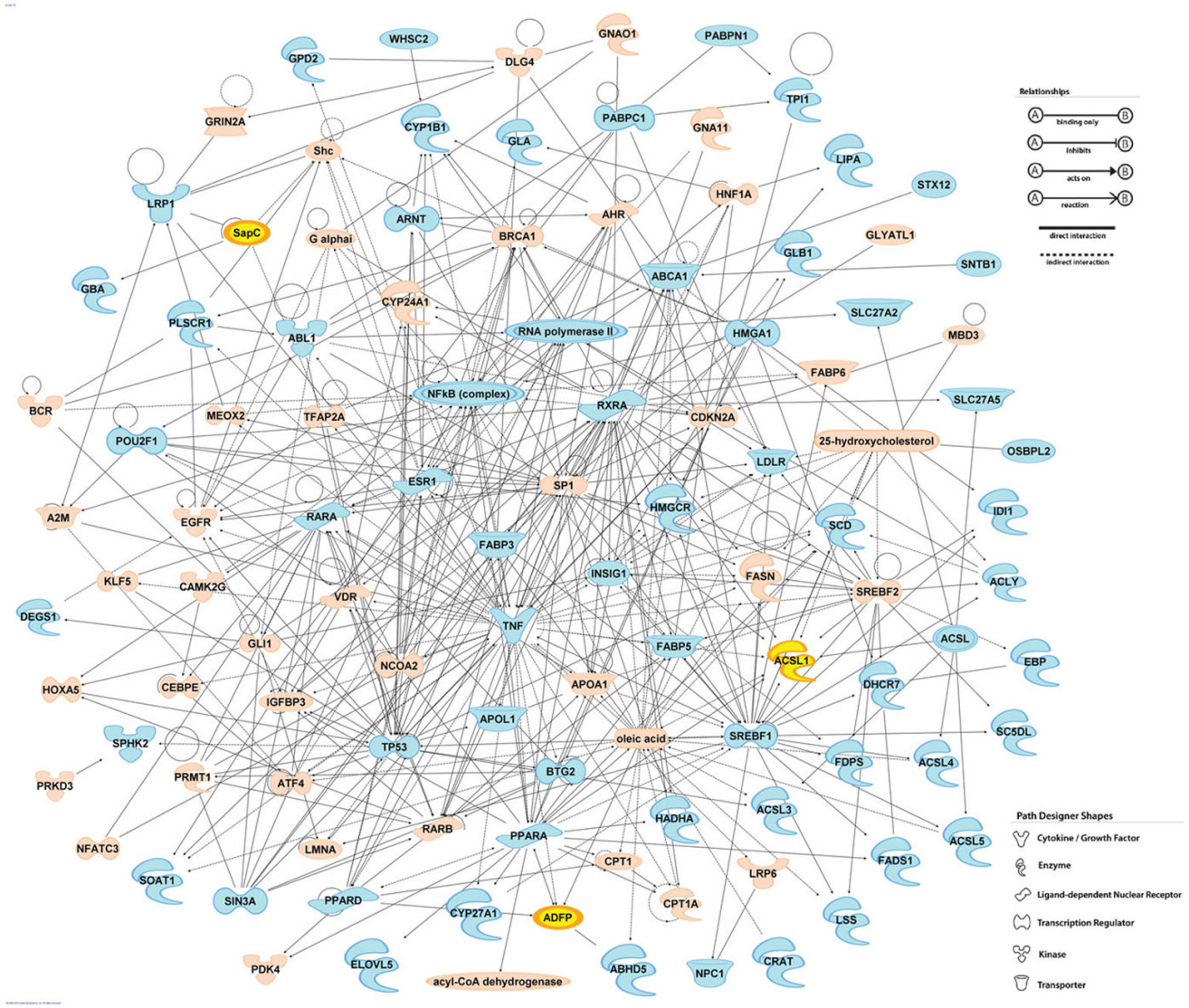

Figure 1. The network of genes involved in lipid metabolism

Genes in blue were upregulated in caseous human pulmonary TB granulomas (Table II), and their relationship was generated by using Ingenuity Pathway Analysis program. *ADFP*, *ACSL1*, and *PSAP* (SapC) are highlighted in yellow. B The genes in pink were either not up-regulated or did not generate statistically significant values ($P < 0.05$)

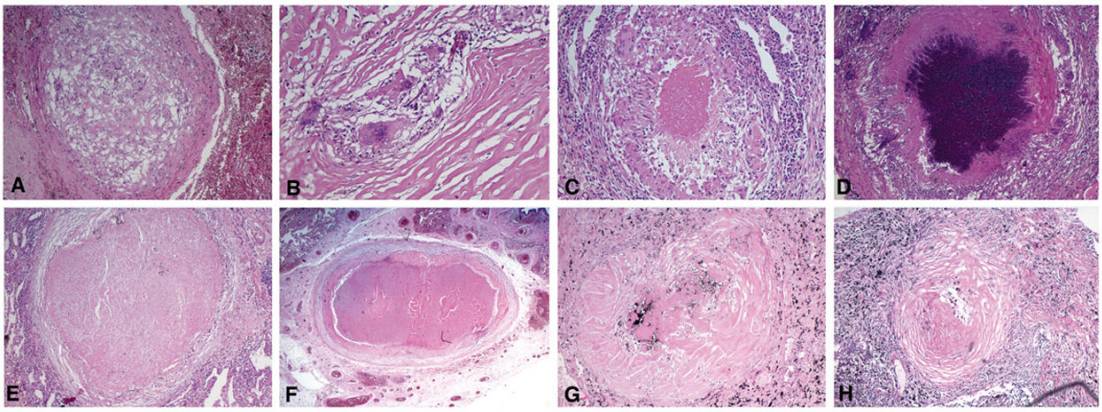

Figure 2. Human TB lung Granulomas at each stage

Human TB lung granulomas were categorized into nascent (**A**: ×40 and **B**: ×100), caseous (**C**: ×100, **D**: ×40), fibrocaseous (**E** and **F**: ×40), or resolved granulomas (**G** and **H**: ×40), and representative images are shown.

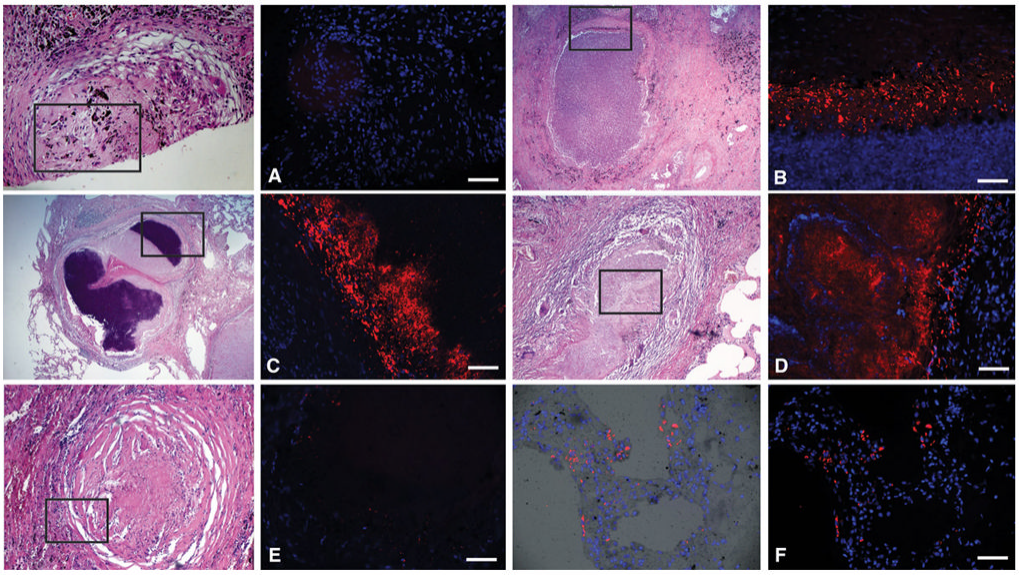

Figure 3. ADFP expression in human TB granulomas

Immunofluorescence signals were obtained for each granuloma, and a representative image (right) and the corresponding area from an H&E slide (left, boxed) are shown. Nuclei are seen in blue and antigens in red. ADFP expression is weak in nascent granulomas **(A)** and resolved granulomas **(E)**. ADFP is strongly expressed in caseous **(B)** and fibrocaseous **(C)** granulomas. Moreover, the caseous center also has intense ADFP expression, together with nuclear debris **(D)**. Control normal lung parenchyma shows ADFP expression in pneumocytes and alveolar macrophages **(F**, the left is a merged image with bright field). Scale bar is 50 μm.

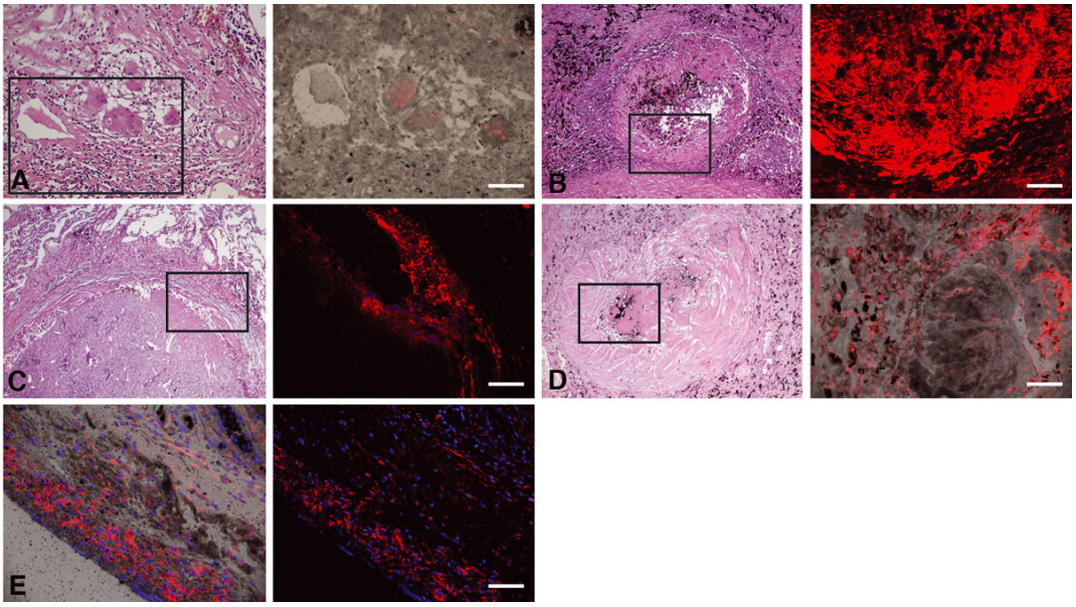

Figure 4. ACSL1 expression in human TB granulomas

Immunofluorescence signals were obtained for each granuloma, and a representative image (right) and the corresponding area from an H&E slide (left, boxed) are shown. Nuclei are seen in blue and antigens in red. ACSL1 expression is weak in nascent granulomas **(A)** and resolved granulomas **(D)**. ACSL1 is strongly expressed in caseous **(B)** and fibrocaseous **(C)** granulomas. Normal lung parenchyma shows ACSL1 expression **(E**, the left is a merged image with bright field). Scale bar is 50 μm.

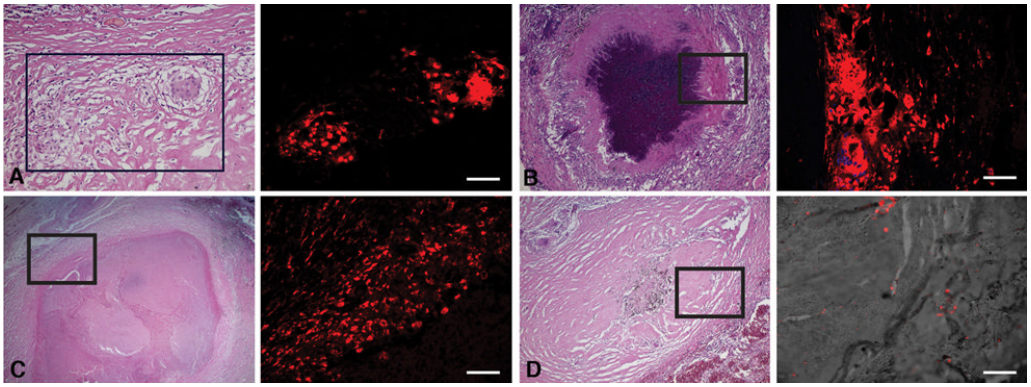

Figure 5. SapC expression in human TB granulomas

Immunofluorescence signals were obtained for each granuloma, and a representative image (right) and the corresponding area from an H&E slide (left, boxed) are shown. Nuclei are seen in blue and antigens in red. SapC is expressed in nascent granuloma **(A)**, caseous granulomas **(B)**, and fibrocaseous **(C)** granulomas. Resolved granulomas show weak expression **(D).** Scale bar is 50 μm.

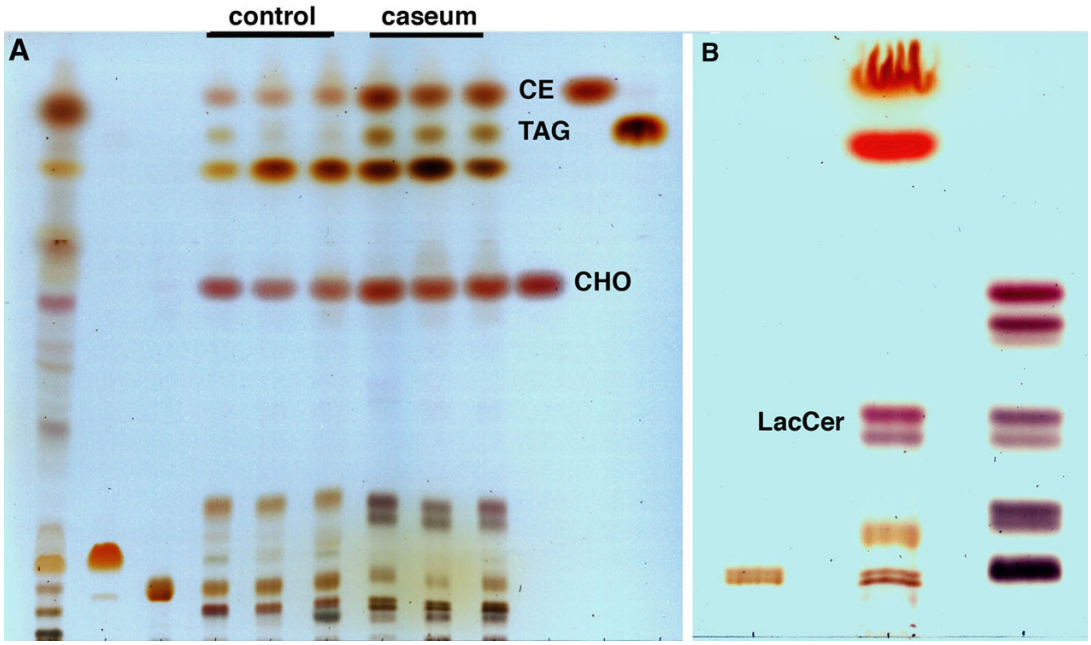

Figure 6. Thin-layer chromatographic analysis of lipids from the caseum and normal lung tissues

Total lipids were extracted from normal lung tissues (lane 4–6, 120 μg) and caseous TB lung granulomas (lane 7–9, 120 μg), and then equivalent amounts were run in parallel with total lipids from Mtb CDC1551 (lane 1, 400 μg), and standard lipids, cardiolipin (lane 2, 50 μg), phosphatidylcholine (lane 3, 50 μg), CHOL (lane 10, 20 μg), CE (lane 11, 25 μg), TAG (lane 12, 20 μg). The caseum reveals an abundance of CHOL, CE, and TAG (**A,** dual solvent system). In addition, the caseum contains lipid species with similar migration to the sphingolipids, and especially LacCer is highly enriched in the caseum (**B**, single solvent system). Total lipids from the caseum (lane 2, 120 μg) were run together with sphingomyelin standard (lane 1, 5 μg) and neutral glycosphingolipids standard (lane 3, 30 μg). Caseous and fibrocaseous granuloma samples were derived from seven independent tissue samples, and normal lung tissue samples

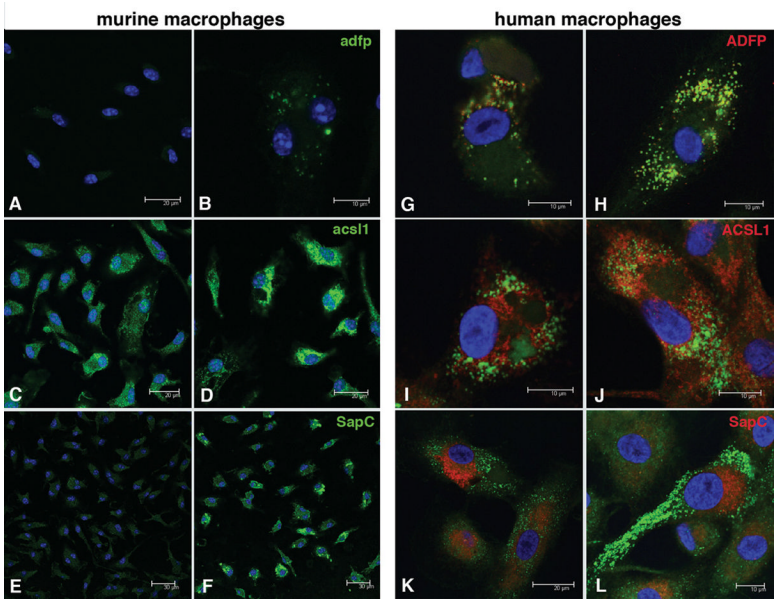

Figure 7. ADFP, ACSL1, and SapC in Mtb-infected macrophages

Murine bone marrow-derived macrophages were infected by Mtb H37Rv for one day, and expressions of Adfp (**A**: control, **B**: Mtb-infected), Acsl1 (**C**: control, **D**: Mtb-infected), and SapC (**E**: control, **F**: Mtb-infected) were examined by confocal microscopy. Blue, nuclei, Green: antigens. Human PBMC-derived macrophages were infected by Mtb H37Rv for four days, and the antigens were detected by confocal microscope. ADFP is tightly associated with lipid droplets (**G**: control, **H**: Mtb-infected), and ACSL1 is also detected along with lipid droplets (**I**: control, **J**: Mtb-infected). SapC is expressed throughout the cytoplasm (**K**: control, **L**: Mtb-infected). Lipid droplets were observed even in uninfected human PBMC-derived macrophages (**G**). Blue: nuclei, red: antigens, green: lipid droplets

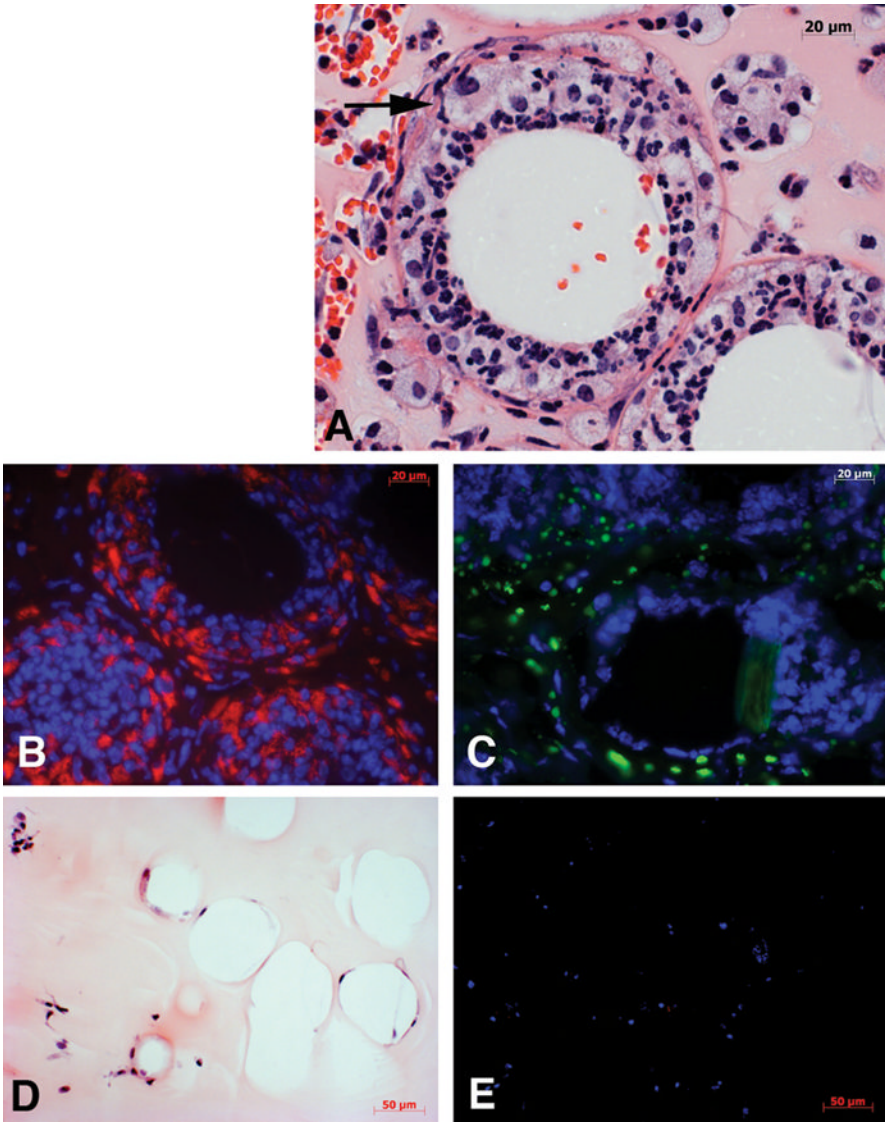

Figure 8. TDM-coated beads induce foam cell formation in mice in an experimental granuloma model

TDM-coated beads resuspended in Matrigel were subcutaneously injected to wild-type mice and the granulomas were excised at day6 post-inoculation. Histological examination demonstrated the extensive recruitment of cells to TDM-coated beads (**A**, H&E), and many of them are lipid droplets-filled foam cells (A representative cell is marked with an arrow). Immunohistology on the consecutive section of the same tissue block for **(A)** revealed a strong expression of lipid droplet-associated protein, Adfp (**B**, nuclei in blue and Adfp in red). Lipid droplets were detected by staining neutral lipids with Nile Red on cryosections from TDM-induced granuloma (**C**, nuclei in blue and neutral lipids in green). In contrast, control lipid PG-coated beads demonstrated considerably reduced recruitment of cells and no induction of foam cell formation (**D**, H&E). Moreover, probing with anti-Adfp antibody on the consecutive section of the same tissue block for **(D)** did not label any of the cells surrounding the PG-coated beads (**E**, nuclei in blue and Adfp in red). The experiments were repeated three times, and three mice were used for PG- or TDM-Matrigel mixture injection.

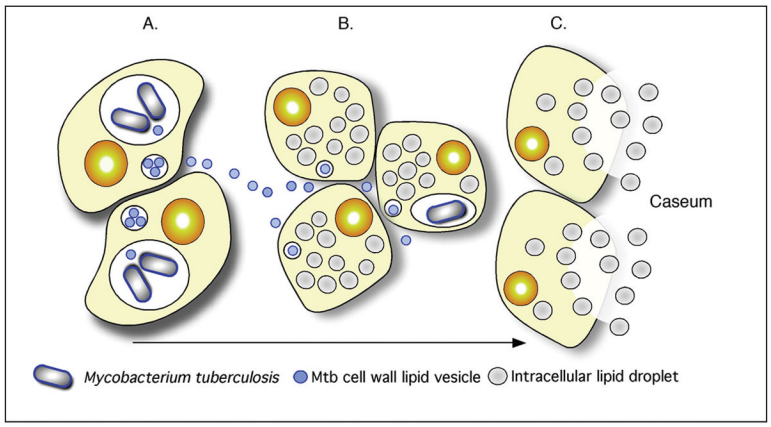

Figure 9. A model illustrating the linkages between Mtb-infection, foam cell formation and accumulation of caseum in the human TB granuloma

A Intracellular Mtb bacilli synthesize and release cell wall components inside their host cells. We have demonstrated previously that these lipids accumulate in the internal vesicles in multi- vesicular bodies, which are exocytosed from the cell in vesicular form. **B** Because of the release of these vesicles, both infected and uninfected macrophages are exposed to cell wall mycolates and induced to form foamy macrophages, as illustrated in Figure 7. The foamy macrophages have been shown to support the maintenance and growth of persistent bacteria. **C** We now propose that these cells die via an inflammatory, necrotic process and release their lipid droplets into the extracellular milieu within the granuloma. As a result of the fibrotic capsule, the human granuloma is an enclosed, isolated structure with minimal vasculature. The enclosed nature of the human granuloma leads to accumulation of necrotic debris as caseum. In this model, this process is an integral part of the pathology that leads to active disease and transmission.

Table I

Genes encoding enzymes involved in lipid metabolism.

Gene	description	Hierarchical Signal Intensity[1]	Fold change[2]	Function
ABHD5	Abhydrolase domain containing 5	9.6	34.3	Triacylglycerol metabolism
ACLY	ATP citrate lyase	12.4	22.7	Acetyl-CoA synthesis
ACSL1	Acyl CoA synthetase long chain fatty acid family member 1	12.7	39.4	Fatty acyl-CoA ester synthesis
ACSL3	Acyl CoA synthetase long chain fatty acid family member 3	11.1	71.2	Fatty acyl-CoA ester synthesis
ACSL4	Acyl CoA synthetase long chain fatty acid family member 4	10.5	261.5	Fatty acyl-CoA ester synthesis
ACSL5	Acyl CoA synthetase long chain fatty acid family member 5	11.7	75.5	Fatty acyl-CoA ester synthesis
ADFP	Adipose differentiation-related protein	13.1	19.1	Lipid accumulation
CRAT	Carnitine O-acetyltransferase	10.6	14.8	Acyl CoA/CoA regulation
CYP1B1	Cytochrome P450, family 1, subfamily B, polypeptide 1	13.6	36.5	Sterol synthesis
CYP27A1	Cytochrome P450, family 27, subfamily A, polypeptide 1	12.6	48.0	Sterol synthesis
DEGS1	Degenerative spermatocyte homolog 1, lipid desaturase	11.8	180.2	Unsaturated fatty acid synthesis
DHCR7	7-dehydrocholesterol reductase	10.0	8.8	Cholesterol synthesis
EBP	Emopamil binding protein	10.4	18.3	Cholesterol synthesis
ELOVL5	Elovl family member 5, elongation of long chain fatty acids	12.4	36.8	Fatty acid synthesis
FADS1	Fatty acid desaturase 1	12.2	45.0	Fatty acid synthesis
FDPS	Farnesyl diphosphate synthase	11.2	8.6	Cholesterol synthesis
GBA	Glucosidase, beta, acid	11.6	32.0	Sphingolipid metabolism
GLA	Galactosidase, alpha	13.0	152.5	Sphingolipid metabolism
GLB1	Galactosidase, beta 1	11.4	19.9	Sphingolipid metabolism
GPD2	Glycerol-3-phosphate dehydrogenase 2	10.2	60.9	Glycerophospholipid metabolism
HADHA	Hydroxyacyl-Coenzyme A dehydrogenase/3-ketoacyl-Coenzyme A thiolase/enoyl-Coenzyme A hydratase, alpha subunit	11.0	16.7	Fatty acid metabolism
HMGCR	3-hydroxy-3methylglutaryl-Coenzyme A reductase	8.9	38.4	Cholesterol synthesis
IDI1	Isopentenyl-diphosphate delta isomerase 1	10.9	7.3	Cholesterol synthesis
LIPA	Lipase A, lysosomal acid, cholesterol esterase	12.6	209.6	Sterol metabolism
LSS	Lanosterol synthase	11.0	8.1	Cholesterol synthesis
PLSCR1	Phospholipid scramblase 1	11.8	137.1	Regulation of lipid accumulation
PSAP	Prosaposin (precursor of sapC)	14.6	30.0	Sphingolipid metabolism
SCD	Stearoyl-CoA desaturase	13.1	76.8	Fatty acid synthesis
SC5DL	Sterol-C5-desaturase	10.1	18.7	Cholesterol synthesis
SOAT1	Sterol O-acyltransferase 1	10.3	47.2	Cholesterol esterification
SPHK2	Sphingosine kinase 2	11.6	32.1	Sphingolipid metabolisum

Gene	description	Hierarchical Signal Intensity[1]	Fold change[2]	Function
TPI1	Triosephosphate isomerase 1	12.4	10.9	Fatty acid synthesis

[1] Gene expression profiles from three independent caseous human TB granulomas were averaged, and the hierarchy of the absolute expression levels was generated.

[2] Gene expression profiles from three independent caseous human TB granulomas were averaged, and then compared to that of normal lung tissue sample. The upregulation of *selected genes* were statistically significant ($P < 0.05$)

Table II

Expressions of *ADFP*, *ACSL1*, and *PSAP* (SapC) are induced by Mtb infection

Gene	Fold induction	
	Murine BMMΦ	Human PBMM
ADFP	2.95	1.22
ACSL1	32.67	1.86
SapC	2.28	1.37

Murine and human macrophages were infected with Mtb H37Rv and mRNA levels of *ADFP*, *ACSL1*, and *PSAP* (SapC) were determined by quantitative real-time RT-PCR. Three technical replicates were included for all conditions and genes. The fold change was calculated using the formula, $2^{-\Delta\Delta Ct}$, and the average of replicates is shown here.